

Exclusive analysis of multiparticle production in π^- -nucleon interactions at 360 GeV/c

Hirotsada Nanjo

Department of Physics, Faculty of Science, Hirosaki University, Hirosaki, 036 Japan

(Received 8 March 1991)

In order to study the detailed structure of the soft component in multiparticle production, an emulsion chamber was exposed to 360-GeV/c π^- beams at CERN, and an exclusive analysis was performed for each interaction. The mutual correlations between the mean value of pseudorapidity, the standard deviation from the mean value, the rapidity density, and the multiplicity in each interaction event were obtained.

PACS number(s): 13.85.Hd

The multiparticle production process cannot be calculated by QCD because of a coupling constant too large for ordinary perturbation theory. Most of the current simulation methods used for the analysis of multiparticle production are based on scaling laws, that is, the Feynman [1] and Koba-Nielson-Olesen (KNO) [2] scaling laws and the fixed P_t distribution. These scaling laws, however, are based on the inclusive or semi-inclusive analysis and do not necessarily reflect the feature of individual interactions.

According to the exclusive analyses of accelerator data [3,4] done to date, small-multiplicity events show an abundance of the asymmetry, and the structure of multiple-meson production changes drastically by its multiplicity. These phenomena cannot be explained by the fluctuation of a model based on inclusive data.

In order to study the detailed structure, we made an exclusive analysis of the multiparticle production process by use of the emulsion chamber exposed to 360-GeV/c π^- beams at CERN. The analysis was made for individual events of the interaction and the many correlations between various physical quantities were examined.

The detector used in this experiment is an emulsion chamber which consists of a multilayered sandwich of nuclear emulsion plates and lead plates. The emulsion chamber is divided into two parts: one is a producer part and the other is an analyzer part. The producer part is composed of a stack of 20 nuclear emulsion plates, which is coated with 150- μm -thick emulsion on both surfaces of 220- μm -thick meta-acryl plate. The analyzer part is for the detection of electron pairs induced by π^0 decay, and consists of an alternate stack of emulsion plates and lead plates (thickness 1 mm) as is illustrated in Fig. 1. The surface area of the chamber is $8.0 \times 9.5 \text{ cm}^2$. This emulsion chamber was vertically exposed to 360-GeV/c π^- beams at CERN with the average flux density of $1.12 \times 10^5 \text{ particle/cm}^2$.

The scanning of events was carried out at each plate by the general scanning method under a microscope. Tracks emitted with large angles were detected carefully in the emulsion just under the interaction point. The tracks with a small angle were followed into two or three downstream layers. The emitting angle of all the secondaries is determined by the geometrical reproduction of the loca-

tion of spots on the different plates which are measured by using the reference tracks of other beams.

The purpose of our investigation is a study of multiparticle production by π^- -nucleon interactions. For this purpose, only events interacted in acryl plates were selected, and the events having heavy tracks were excluded. Under these selections, 194 events were obtained.

In the case of acryl jets, the interaction points cannot be seen directly. This effect brings some biases not only in the scanning of events but also in the detection of tracks. As regards the detection of tracks, the particles emitted with large angle tend to be missed. The limit of the detection angle is estimated as about 60° ($\eta \approx 0.5$) in the laboratory system.

In the general scanning method, the events of low multiplicity have a tendency to be missed. The half-angle in the case of π^- -p 360-GeV/c interaction is 4° in the laboratory system, which corresponds to the distance of 16 μm from the center of the jet showers at most. The scanning bias, therefore, can be found only for the events of low multiplicity and with large emitting angle.

The multiplicity n_{ch} distribution is shown in Fig. 2, where it can be compared with the result of 360-GeV/c π^- -p bubble-chamber data [5]. Our result gives a scarce distribution at low multiplicity ($n_{\text{ch}} \leq 4$) because of the

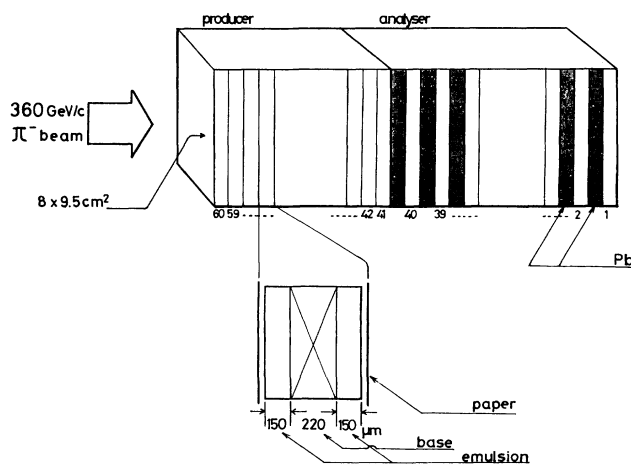


FIG. 1. The design of the detector.

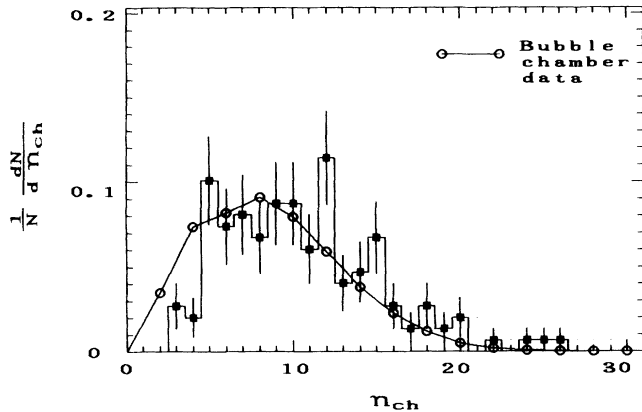


FIG. 2. The multiplicity of the n_{ch} distribution. Open circles represent the result of the 360-GeV/c π^-p bubble-chamber data.

scanning bias as mentioned above. The enhancement at high multiplicity is not so large and this fact gives us the estimation that the nucleus effect by a target is not so large.

The pseudorapidity η^* in the c.m. system (c.m.s.) ($\eta^* = \eta - 3.32$) distribution is shown in Fig. 3, classified by multiplicity. The large inclination toward the forward direction in low-multiplicity events ($n_{ch} \leq 5$) is due not only to a large contribution of leading particle [6], but also the scanning bias that events having large-angle tracks tend to be missed. The enhancement in the backward direction by the nucleus effect can be seen slightly only for the events of $n_{ch} \geq 17$.

The total rapidity Y^* distribution is shown in Fig. 4. The distribution of the $\pi^- + p \rightarrow \pi^\pm + X$ 205-GeV/c data [7] in the figure is widened to the case of the 360-GeV/c interaction according to the scaling law (because of none of the data in 360 GeV/c). In this figure, the value of pseudorapidity η^* is transformed to the value of rapidity Y^* . The scarce distribution in the backward region ($Y^* < -2.5$) is due to the detection bias as mentioned

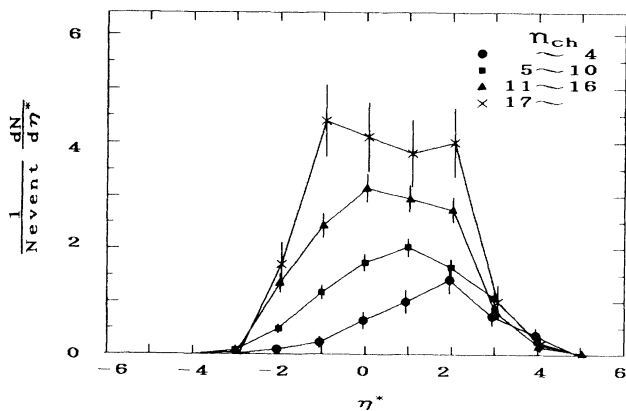


FIG. 3. The pseudorapidity η^* density distributions classified by the multiplicity. The \bullet , \blacksquare , \blacktriangle , and \times marks are for $n_{ch} \leq 4$, $5 \leq n_{ch} \leq 10$, $11 \leq n_{ch} \leq 16$, and $n_{ch} \geq 17$, respectively.

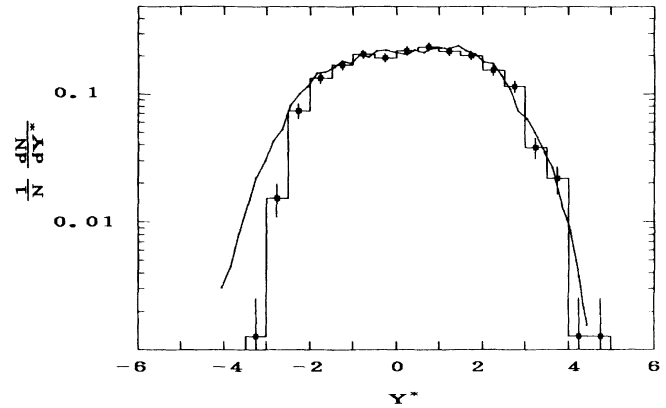


FIG. 4. The Y^* distribution for the events of $n_{ch} \geq 5$. The solid curve represents the result of $\pi^- + p \rightarrow \pi^\pm + X$ data.

above. The result shows a good agreement with the bubble-chamber data except in the region of $Y^* < -2.5$.

The above results show that the scanning bias is restricted in the low-multiplicity events of which tracks concentrate into the backward direction. As regards the nucleus effect, the results represent scarce influences within the limitation of the detection angle $Y^* \approx -2.5$. The analysis was carried out after due consideration of these biases.

The purpose of our investigation is to study the feature of pionization, which is the residual part taking away leading and recoil particles in individual events. In this work, we assume that a track with the maximum rapidity η^* is of a leading particle and all of other tracks are secondary particles from the pionization. Recoil protons are ignored for the reason that half the recoil nucleons should be neutrons and recoil nucleons do not always have the minimum value of η^* by the effect of the mass difference between the π meson and nucleon.

Figure 5 shows the rapidity Y^* distribution removing the leading and recoil particles, compared with the

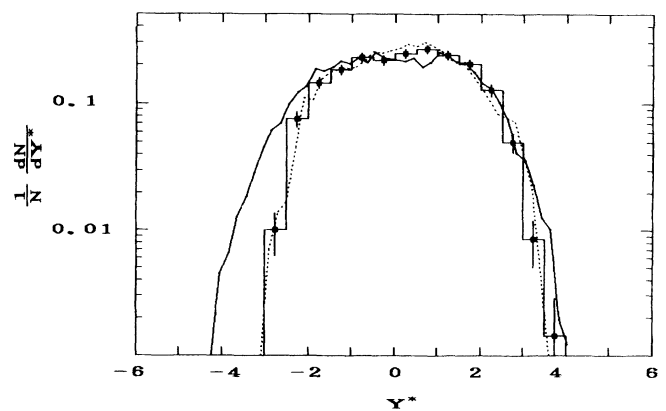


FIG. 5. The Y^* distribution removed tracks with the maximum Y^* in each interaction. The solid curve and dotted line represent the result of $\pi^- + p \rightarrow \pi^\pm + X$ data and $\pi^- + p \rightarrow \gamma + X$ data, respectively.

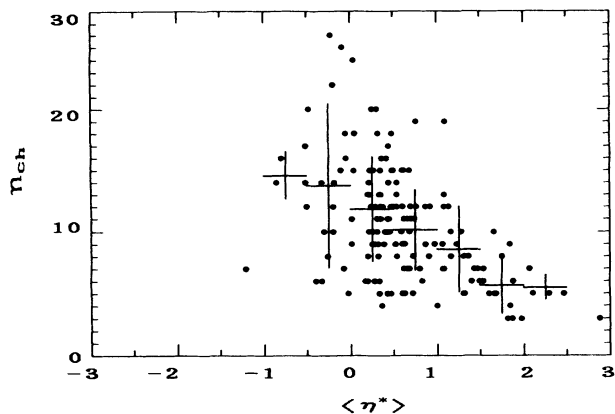


FIG. 6. The correlation between $\langle \eta^* \rangle$ and n_{ch} . The horizontal and vertical lines represent the mean value and standard deviation, respectively.

$\pi^- + p \rightarrow \pi^+ + X$ 205-GeV/c data [7] and the $\pi^- + p \rightarrow \gamma + X$ 360-GeV/c data [8]. The distribution of the 205-GeV/c data is also widened according to the scaling law. Since the π^+ and γ particles should be free from the leading and recoil particles, the good agreement with the π^+ and γ data indicates that the tracks removing the minimum η^* track reproduce the pionization particles. The difference between the π^+ and γ data in the backward region ($Y^* < -2.5$) is considered to be due to the scanning bias of the γ ray in the same way as our measurement.

In order to investigate the feature of pionization, the mean value of pseudorapidity $\langle \eta^* \rangle$, the standard deviation σ from $\langle \eta^* \rangle$, and the density ρ in a unit η^* are obtained in each interaction event, as follows:

$$\langle \eta^* \rangle = \sum \eta_i^* / n_{pz}, \quad (1)$$

$$\sigma = \sqrt{\sum (\eta_i^* - \langle \eta^* \rangle)^2 / (n_{pz} - 1)}, \quad (2)$$

$$\rho = 0.6827 \times n_{pz} / 2\sigma, \quad (3)$$

where n_{pz} is the number of tracks in the pionization, and the factor of 0.6827 means the probability in $\pm 1\sigma$ width in the case of Gaussian distribution.

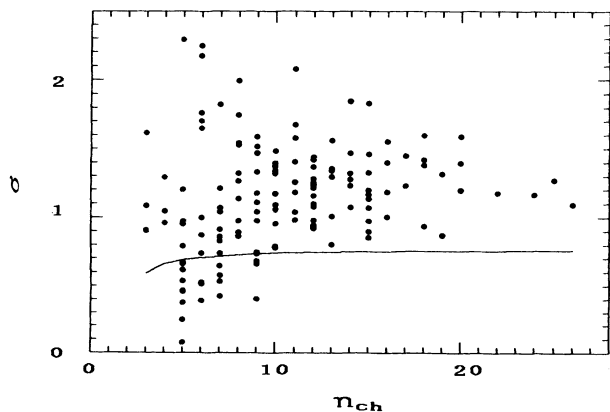


FIG. 7. The correlation between n_{ch} and σ . The solid curve represents the correlation in the case of isotropic decay by the simulation data.

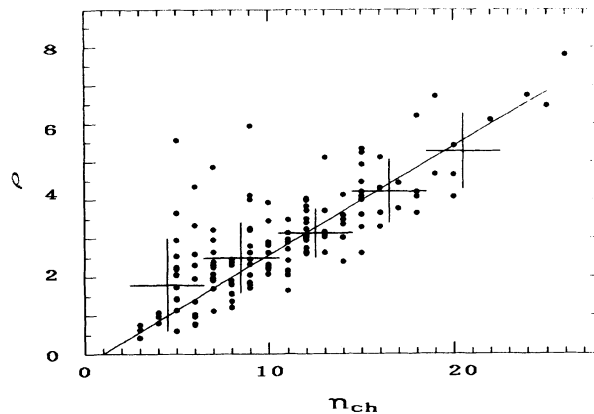
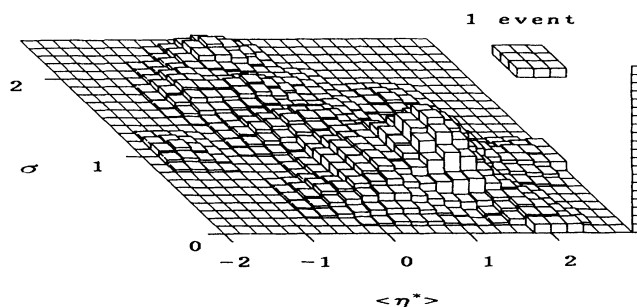


FIG. 8. The correlation between n_{ch} and ρ . The straight line represents the correlation in the case of a constant σ of 1.1.

The correlation between $\langle \eta^* \rangle$ and n_{ch} is shown in Fig. 6. The $\langle \eta^* \rangle$ value is distributed symmetrically around zero in the case of high-multiplicity events ($n_{ch} > 10$). The low-multiplicity event, on the contrary, is inclined toward a positive value of $\langle \eta^* \rangle$, and the lack in the negative range is considered to be caused by the scanning bias of events, as mentioned above.

(a) $n_{ch} \leq 8$



(b) $n_{ch} \geq 9$

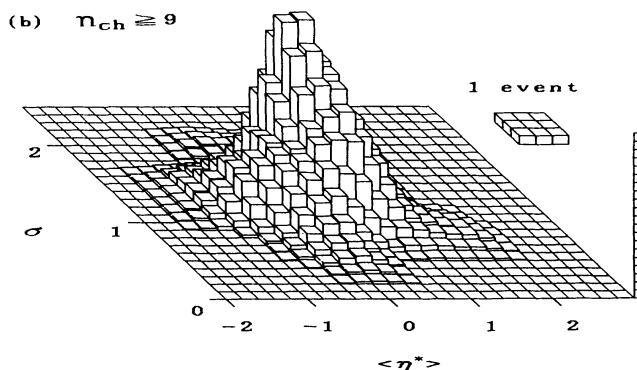


FIG. 9. The cell distribution as a function of $\langle \eta^* \rangle$ and σ , (a) is for $n_{ch} \leq 8$ and (b) is for $n_{ch} \geq 9$. The histogram is smoothed for the reason of scarce statistics.

Figure 7 shows the correlation between σ and η_{ch} . This figure also shows the different features between low-multiplicity ($n_{\text{ch}} < 8$) and high-multiplicity events. The value of σ for the low-multiplicity events is divided into two groups: one is nearly equal to the value of isotropic decay (solid curve), and the other is nearly equal to 2. In the case of high-multiplicity events, the value is larger than in the isotropic decay and remains constant. The excess of the events in the region of small σ (< 2) and small n_{ch} ($n_{\text{ch}} < 10$) contradicts the mutual independence of Feynman and KNO scaling laws which are widely adopted in the current simulation methods.

The correlation between ρ and n_{ch} is shown in Fig. 8. The result shows that they are roughly in proportion to each other, except in the small- n_{ch} region. This result indicates that the increase of the multiplicity is mainly due to the increase of the rapidity density.

The direct correlation between $\langle \eta^* \rangle$ and σ classified

with the multiplicity is shown in Fig. 9. The height in this figure represents the smoothed frequency. As is shown in this figure, the high-multiplicity events concentrate in the region of large σ (≈ 1.2) and $\langle \eta^* \rangle \approx 0$. The low-multiplicity events have a small σ (≈ 0.8) and large $\langle \eta^* \rangle$ (≈ 1.2) value, but there also can be seen a group in the region of large σ and $\langle \eta^* \rangle \approx 0$. The asymmetry in $\langle \eta^* \rangle$ (the lack of a peak in minus $\langle \eta^* \rangle$) is not caused by the detection bias of a large angle, but is caused by the scanning bias, as mentioned above.

The author would like to express his gratitude to the members of CERN for making successful exposures of the emulsion chamber to accelerator beams. The author is also indebted to A. Saito at Towadanishi High School, Y. Noto at the Japan Meteorological Agency, and other members of our laboratories for their valuable discussions and the contribution in scanning and measuring.

-
- [1] R. P. Feynman, *Phys. Rev. Lett.* **23**, 1415 (1969).
 - [2] Z. Koba, H. B. Nielsen, and P. Olesen, *Nucl. Phys.* **B40**, 317 (1972).
 - [3] H. Nanjo and K. Tanaka, *Prog. Theor. Phys. Suppl.* **54**, 120 (1973).
 - [4] Y. Hayashi, H. Nanjo, and K. Takitani, *Sci. Rep. Hiroasaki Univer.* **28**, 23 (1981).
 - [5] J. Whitmore *et al.*, *Phys. Rev. D* **16**, 3137 (1977).

- [6] A. Firestone *et al.*, *Phys. Rev. D* **14**, 2902 (1976).
- [7] V. P. Kenney, in *Particles and Fields—1975*, Proceedings of the Annual Meeting of the Division of Particles and Fields of the APS, Seattle, Washington, 1975, edited by H. J. Lubatti and P. M. Mockett (Physics Department, University of Washington, Seattle, 1975), p. 254.
- [8] N. N. Biswas *et al.*, *Nucl. Phys.* **B167**, 41 (1980).

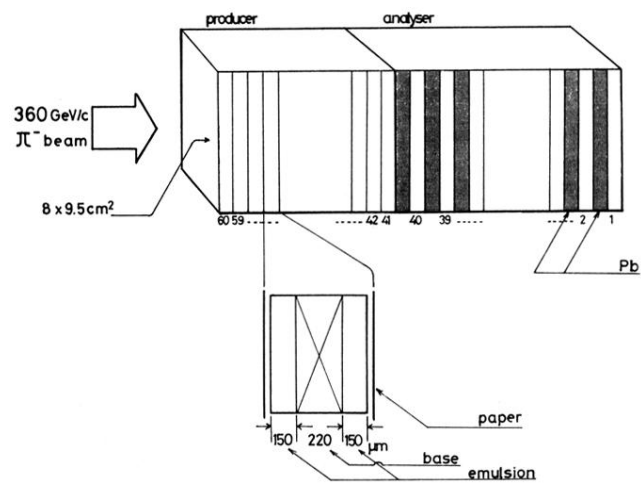


FIG. 1. The design of the detector.